Images as Symbols: An Associative Neurotransmitter-Field Model of the Brodmann Areas

Douglas S. Greer

General Manifolds
Carlsbad, California, USA
dsgreer@gmanif.com

Abstract. The ability to associate images is the basis for learning relationships involving vision, hearing, tactile sensation, and kinetic motion. A new architecture is described that has only local, recurrent connections, but can directly form global image associations. This architecture has many similarities to the structure of the cerebral cortex, including the division into Brodmann areas, the distinct internal and external lamina, and the pattern of neuron interconnection. The images are represented as neurotransmitter fields, which differ from neural fields in the underlying principle that the state variables are not the neuron action potentials, but the chemical concentration of neurotransmitters in the extracellular space. The neurotransmitter cloud hypothesis, which asserts that functions of space, time and frequency, are encoded by the density of identifiable molecules, allows the abstract mathematical power of cellular processing to be extended by incorporating a new chemical model of computation. This makes it possible for a small number of neurons, even a single neuron, to establish an association between arbitrary images. A single layer of neurons, in effect, performs the computation of a two-layer neural network.

Analogous to the bits in an SR flip-flop, two arbitrary images can hold each other in place in an association processor and thereby form a short-term image memory. Just as the reciprocal voltage levels in a flip-flop can produce a dynamical system with two stable states, reciprocal-image pairs can generate stable attractors thereby allowing the images to serve as symbols. Spherically symmetric wavelets, identical to those found in the receptive fields of the retina, enable efficient image computations. Noise reduction in the continuous wavelet transform representations is possible using an orthogonal projection based on the reproducing kernel. Experimental results demonstrating stable reciprocal-image attractors are presented.

Keywords: Natural intelligence, computational neuroscience, cognitive signal processing, memory, pattern recognition, neurotransmitter fields.

Transactions on Computational Science V, LNCS 5540, pp. 38–68, 2009.
M.L. Gavrilova et al. (Eds.) Springer-Verlag

1 Introduction

Throughout its entire extent, the cerebral cortex is composed of the same six cellular layers. Based on the relative thickness of these layers, Brodmann divided the cerebral cortex of humans into approximately fifty areas [1]. His illustration, shown in Fig. 1, was originally published one hundred years ago, but is still used in neuroscience textbooks today [2], [3]. Between Brodmann areas, the cortical layers vary in thickness, but within each area, they are roughly the same. At the boundaries between areas, there is a sharp and sudden change in the relative prominence of the six cellular lamina.

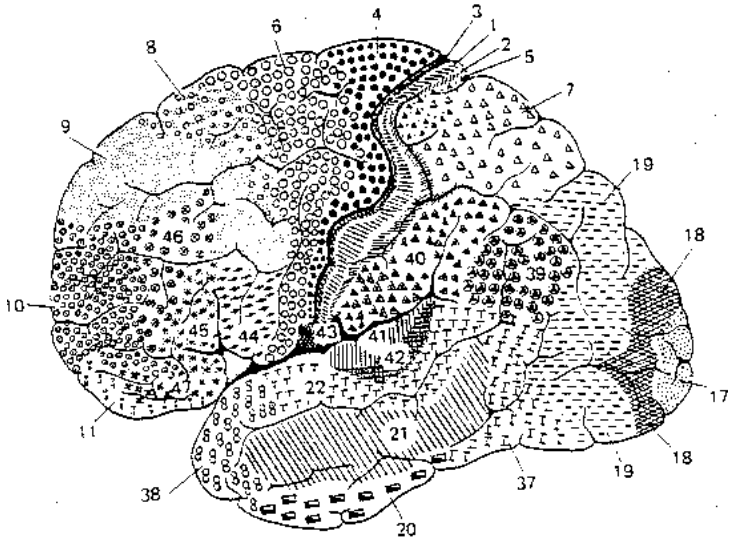

Fig. 1. Lateral view of the human brain divided into areas from the original work by Brodmann. The boundaries between the Brodmann areas are determined by the thickness of the six cellular layers.

A cross section of the neocortex, first published by Brodmann and Vogt, is shown as the background illustration in Fig. 2. The six cellular layers are labeled I through VI. Layers II and IV are the *external and internal granule* layers respectively, while layers III and V are the *external and internal pyramidal* layers. In addition, on the right side of Fig. 2, which has been prepared with a Weigert stain, the *external and internal Bands of Baillarger*, labeled 4 and 5b are visible. A complete theory of natural intelligence must somehow account for this uniform structure, and the existence of the two nearly identical (external and internal) parallel systems.

Also shown in the center of Fig. 2 is a loop representing a cortical column created from the local connections between neurons in the various layers. Even though most neurons have a width of only a few microns, they form layers of constant thickness over the full extent of the Brodmann areas, which may be several square centimeters in size. These facts are consistent with an image association model.

We use the term *image* or *field* in a general mathematical sense for a scalar or vector valued function defined on a manifold [4], [5], for example an open region of the plane $(\mathbb{R}^2)$. We use script letters to denote function transforms, for example the wavelet transform of a function f is written as $\mathcal{W}[f]$.

Each layer of each Brodmann area can be considered to be one image. Consequently, the general notion of an image plays a role in cognition that extends beyond computer vision. For example, we can model an audio spectrogram that represents time in the horizontal dimension and frequency in the vertical dimension as a two-dimensional image. Similar tonotopic maps exist at several locations in the central nervous system (CNS) [2], [6].

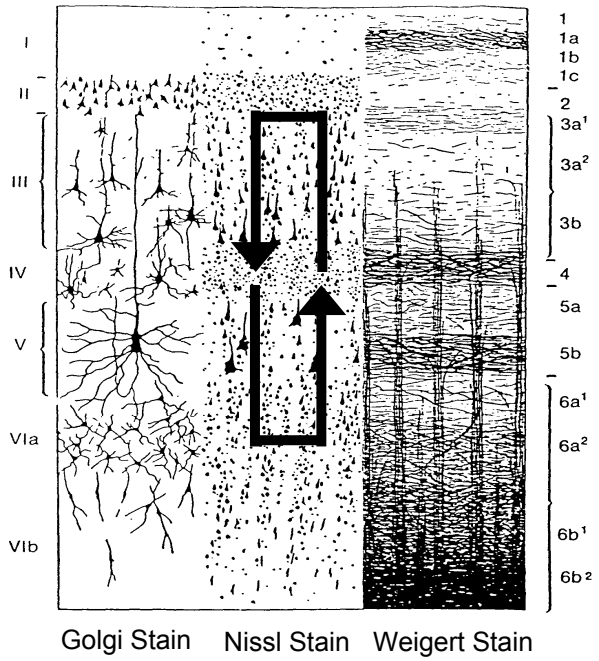

Fig. 2. A cross-section of the cerebral cortex showing the six cellular layers. Most of the structures occur in external/internal pairs such as the granular layers (II and IV), the pyramidal layers (III and V) and the Bands of Baillarger (4 and 5b). The loop in the center depicts the connections of a single cortical column. (background from Brodmann & Vogt, 1908).

The generalization of images to include any function defined on a manifold is a powerful one in terms of its ability to describe and model many natural phenomena. Images can include mass (external world), position (location of the body surface), energy (visible light and sound vibrations), and force (pressure on the body surface, or the tension on the combined muscle cross-sections).

For example, the surface of the skin (a somatotopic map) can be modeled as a two-dimensional manifold, and its position in space then becomes a vector valued function defined on that surface. A manifest of the two-dimensional images that are

processed by the CNS is extensive [7], and includes retinotopic maps, spatial maps, and kinetic maps.

In this context, learning and retrieving image associations can be viewed as a basic cognitive function. As an example, when children learn a new word, say "horse", they learn to associate two images: the visual image of a picture of a horse and the two-dimensional audio spectrogram of the sound of the word "horse".

An assumption of the standard neural-network perceptron model is that the electrical action potentials are the information, and neurotransmitters serve only as a mechanism for transferring a weighted response between neurons. However, if we step back and allow ourselves to view the neurotransmitter concentration as the data, a different model of computation emerges.

Information and computation are mathematical abstractions and can be realized by many different physical means. For example, mechanical computing devices have a long history that predates the discovery of electricity. In complex biological organisms, cellular signaling generally takes place using chemical mechanisms. If a limb of a tree is removed, the tree will grow a new one with the all the detailed structure necessary to create the leaves and branches. This massive computation takes place without electricity. The chemical signals employed in this computation are virtually identical to the substances used as neurotransmitters in the brain.

To survive, an organism must maintain efficient and accurate representations of force, mass, energy, and other functions of time, space, and frequency. We can imagine a compact, high-resolution data representation analogous to ink on a sheet of paper. The neurotransmitter "ink" is written and erased by the axons and "read" by the dendrites. We explore this new model of natural computation where the data itself is chemical rather than electrical. The information is encoded by the molecular density of neurotransmitter that is released by multiple axons into the synaptic cleft.

Modeling a large number of particles with integral and differential equations is common in physics. Neurotransmitter fields use this same abstraction to model data as a continuous function in three-dimensional space. The need for a continuous rather than discrete cognitive representation also follows from the scientific philosophy described by Monad [8]. As applied to neuroscience, any inconsistencies that may appear due to the discretization of physical laws will tend to be removed by natural selection. Therefore, since space is isotropic and homogeneous, at some level of abstraction the computational model itself should be continuous. Since these calculations may be carried out by many types of biological cells other than neurons, we use the term *computational manifold* to refer to the generalization of discrete neural networks to continuous spaces.

We discuss two types of image association processors. The first of these, the Λ-*map*, is feed-forward and has no recurrent loops. It can however perform logic operations by producing the output image that is associated with multiple input images. The second type of association processor, the *psymap*, is constructed from two Λ-maps and is analogous to a set-reset flip-flop where the individual bits have been replaced by two-dimensional images. Its design uses recurrence to integrate the results of many locally connected processing elements into an overall global image association.

Borrowing from the terminology of digital design, specifically a programmable logic array, the term *psymap array* is used to specify an interconnected collection of psymaps where the bits are again replaced by images.

The coefficients of spectral representations such as wavelets, in effect, encode weighted averages over regions. Spherically symmetric wavelets, similar to the receptive fields of the retina, allow image associations to be computed faster and more efficiently. We hypothesize that these wavelet-like fields are not unique to the visual system but are a general principle of operation that governs the entire cerebral cortex.

The continuous wavelet transform contains redundant information that is characterized by the reproducing kernel [9]. When associations are formed between image spectral representations, this redundant information can be used to reduce errors and increase stability.

The behavior of a psymap over time can be viewed as a dynamical system. We describe an algorithm where two arbitrary images can be linked together to form a *reciprocal image* pair. Each pair can be used to create a *reciprocal-image attractor* where images near an attractor converge toward it.

Symbolic processing is traditionally performed by manipulating bit patterns in a digital computer. We present a new type of symbolic processing where the symbols are images. Whether the symbols are discrete bit patterns or continuous functions, in order to overcome the effects of noise, a necessary condition required to construct actual implementations is that the symbol representations act as stable fixed-points in a dynamical system.

A new software package was written to verify that neurotransmitter-field theory could be used to construct structurally stable reciprocal-image attractors. The computational results shown demonstrate how stable attractor basins can be created around arbitrary image pairs and thereby form the foundation of an image-based symbol processing system.

1.1 Related Work

A psymap array is an implementation of an abstract symbol processing system. Consequently, descriptions of cognitive models that can be expressed in terms of symbolic operations [10], [11] can be used to evaluate psymaps, which use images to represent symbols. Control masks, in particular time-varying control masks, act as instructions for directing the operation of the array. Therefore, the ability to recall control mask images translates into the ability to recall procedures that operate on symbols. Cognitive informatics describes how the acquisition, representation, retrieval, and comprehension of concepts may be expressed as an aggregation of symbols and operators [12], [13]. These theoretical frameworks can be applied in the analysis of psymap arrays as computational engines that evaluate semantic functions.

In contrast to some previous work that uses feature detection and extraction and performs the analysis in a lower dimensional space, we discuss algorithms where the images maintain their topological structure and the associations take place directly between the image wavelet transforms.

Transactions on Computational Science V, LNCS 5540, pp. 38–68, 2009.
M.L. Gavrilova et al. (Eds.) Springer-Verlag

Willshaw [14] first proposed a model of associative memories using non-holographic methods. Bidirectional associative memories were originally proposed by Kosko [15] and subsequently developed by others [16]. These neural networks are designed such that all of the outputs directly depend on all the inputs, that is, they require global connections to the entire input image. Consequently, implementations can suffer from poor performance for high-resolution images or large training sets. Cellular neural networks, first described by Chua and Yang [17], are implemented with local connections, but do not use spectral methods or aggregate multiple images with a unified control structure.

A second type of neural-network associative memory is created by following the trajectory of a particle in a dynamical system governed by a recurrence of the form $\vec{x}_{i+1} = f(\vec{x}_i)$. The association is not fixed in time but is the relationship between a starting point and a final fixed point of the dynamical system. To distinguish between these two types of association mechanisms we will refer to the second type as a classification, where each unique fixed point identifies a *class* that equals the set of all points whose trajectory leads to that point. The psymap model may also go through a classification phase, but once the association is formed, the relationship between the associated images is static and explicit.

Wavelet networks combine the functional decomposition of wavelets with the parameter estimation and learning capacity of neural networks [18]–[20]. However, these differ from the psymap methods in their lack of reciprocal associations formed between representations. Moreover, their use of wavelet basis functions rather than the continuous wavelet transform implies that the projection based on the reproducing kernel will not reduce noise and add stability since the basis functions are by definition linearly independent.

2 Neurotransmitter Fields

Neural fields have been studied for a long time [21]–[24] and comprehensively reviewed by several authors [25], [26]. This approach models the behavior of a large number of neurons by taking the continuum limit of discrete neural networks where the continuous state variables are a function in space representing the mean firing rates.

The distinction between neural fields and neurotransmitter fields is the physical quantity under consideration. Neural fields attempt to model the spatial distribution of mean neuron-firing rates as a real-valued function, while neurotransmitter fields model the concentration of neurotransmitters in the extracellular space as a real-valued function. The localization of neurotransmitters to the space within the synaptic cleft is seen as an evolutionary adaptation that limits diffusion and increases the efficiency.

In order to develop the theory, we put forth a single proposition: the neurotransmitter cloud hypothesis. Empirical evidence and deductive arguments are provided which support this proposition, but verification will require further investigation and analysis. Acceptance of the hypotheses, like including an additional

mathematical axiom, allows us to explore a new computational model that characterizes the electro-chemical properties of the neuron.

2.1 Evolution of the Nervous System

Although the evolution of the senses and the central nervous system was a complex process that occurred over an extended time interval [27], we can attempt to understand some of the general constraints that may have influenced its development. One of these constraints was the need to evaluate the current state of the body and its immediate environment. This required the creation of internal representations that could be equated with physical quantities defined over the continuous variables of space, time, and frequency.

In the standard neural network model, a synapse is characterized mathematically by a single real-valued weight representing the effect one neuron has on another. The products of the weights times the activation values of the input neurons are summed, and a nonlinear transfer function is applied to the result [28]. This model describes electrical and chemical synapses uniformly, that is, by a single real value. Examining the difference between electrical and chemical synapses, we note that electrical synapses, which may have a weighted response proportional to the number of ion channels connecting the pre- and postsynaptic neuron, are more than ten times faster. They are also more efficient, since they do not require the metabolism of neurotransmitters, or the mechanics of chemical signaling. However, chemical synapses are found almost exclusively throughout the central nervous systems of vertebrates. This raises the question: Given a time interval of several hundred million years, and the wide range of species involved, why has nature consistently retained the cumbersome chemical synapses and not replaced them with electrical synapses?

We note that neurotransmitters, the core component of chemical synapses, are actually located outside the neuron cell walls in the extracellular space. Moreover, the chemical signaling often occurs in multiple-synapse boutons such as the one shown in Fig. 3. Within these complex synapses, which connect the axons and dendritic spines of many adjacent neurons, the density of neurotransmitter is equal to the sum of the contributions from each of the individual axons.

Another constraint during the course of evolution was the limited amount of processing power available. Solutions that required more than a very small number of neurons were not feasible. In addition, the space within the organism that could be devoted to representing physical quantities was limited, so small, compact representations were preferable.

If we leave the confines of the standard neuron model and consider the density of neurotransmitters as the state variables, we discover a number of advantages. The first is higher resolution; billions of small molecules can fit in the space occupied by a single neuron. The second is energy consumption; the concentration of neurotransmitters, like the concentration of ink on a sheet of paper, is passive and can store information indefinitely without expending energy. In contrast, action potentials require the continuous expenditure of energy in order to maintain state. Another

advantage is that a very high-resolution representation can be maintained with only a few processing elements. For example, the terminal arbor of a single neuron that encodes a joint angle can support a high-resolution model describing the location of the surface of the limb in space. This collection of related concepts results in the following conjecture.

> **The Neurotransmitter Cloud Hypothesis:** When multicellular fauna first appeared, organisms began to represent quantities such as mass, force, energy and position by the chemical concentration of identifiable molecules in the extracellular space. The basic principles of operation developed during this period still govern the central nervous system today.

The basic laws of physics are based on quantities defined in space, time, and frequency, which can be internally represented by the chemical concentration of neurotransmitters in three-dimensional space.

Neurotransmitter clouds in early metazoa would have suffered from two problems: chemical diffusion of the molecules and chemical inertia due to the large amount of neurotransmitter required to fill in the extracellular space. As a result, evolutionary adaptation would have favored neural structures where the neurotransmitters remained confined to the small regions in the synaptic clefts between the pre- and postsynaptic neurons.

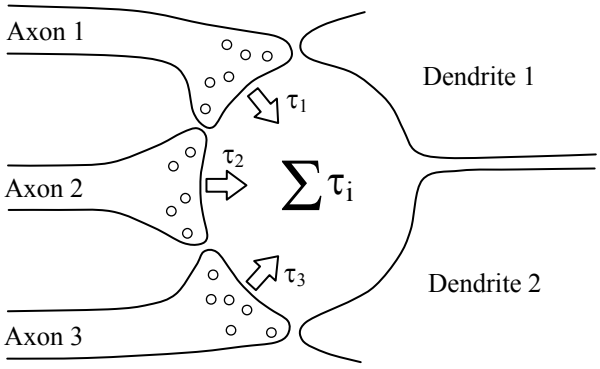

Fig. 3. This idealized view of multi-synapse boutons shows how the concentration of neurotransmitter perceived by multiple dendrites is the summation of that produced by three separate axon terminals. The summation occurs in the extracellular space and is separated from the intracellular summation by the nonlinear responses of the cell membranes.

In order to visualize how a computation can be performed on a neurotransmitter cloud, imagine the dendritic arbor of a neuron as a leafless tree with its branches inside of the cloud. The surface of the tree is "painted" with a shade of gray that corresponds to its sensitivity to a particular neurotransmitter. When multiplied by the actual concentration of neurotransmitter present in the extracellular space, and

integrated over a region of space that contains the dendritic tree, the result is a first-order approximation of the neuron's response. We can mathematically represent the "shade of gray" that corresponds to the sensitivity of a neuron's dendritic arbor in physical space by a function $\mu(x,y,z)$.

2.2 Neurotransmitter Field Theory

The standard projection neural network calculation is based on the inner product of two vectors, a vector of input values, and a weight vector. Hilbert spaces generalize the inner product operation to continuous domains by replacing the summation of the products of the vector coefficients, with the integral of the product of two functions [29]. One of these two functions, $\mu(x,y,z)$, is used to represent the sensitivity of the dendritic arbor and is analogous to the weight vector.

Let H be the three-dimensional space representing a neurotransmitter cloud, and let $h(x,y,z)$ be a field corresponding to the density of transmitter in the extracellular space. We conceptually model the operation of a neuron as an abstract *Processing Element* (PE). The dendritic arbor computation of the PE, which is analogous to the vector inner product, is defined by the integral of h and with respect to μ

$$\text{response} = \iiint_H h(x,y,z)\, d\mu(x,y,z) \tag{1}$$

In [30] it is shown that by using Lebesgue integrals and Dirac delta functions the mathematical formulation of neurotransmitter fields (1) subsumes the functionality of the neural networks. That is, for every neural network, there exists a corresponding neurotransmitter field integral over a dendritic tree that generates an identical result.

Mathematically the neurotransmitter "clouds" are three-dimensional manifolds which we illustrate diagrammatically as rectangular blocks such as the input manifold H and the output manifold G shown in Fig. 4A. To distinguish between the input and output spaces, we substitute the parameters (ξ,η,ζ) for (x,y,z) in the input manifold H.

In addition to the dendritic arbor, each neuron (or astrocyte) also has an axonal tree, or terminal arbor, which releases neurotransmitter into the extracellular space. Let $\tau(x,y,z)$ denote the function that quantitatively describes the output of a neuron in terms of the spatial distribution of chemical neurotransmitter it generates.

We use the index i to enumerate the set of processing elements $\{PE_i\}$. Each processing element, such as the ones shown in Fig. 4A, consists of a unique *receptor measure,* $\mu_i(\xi,\eta,\zeta)$, a *transmitter function* $\tau_i(x,y,z)$ and nonlinear *cell-membrane-transfer functions,* χ and σ. The spatial variations are modeled using μ_i and τ_i and we assume that χ and σ are fixed functions of a single real variable, similar to the sigmoidal transfer functions used in neural networks.

The transformation from a discrete real value back to a continuous field results from scaling the output of the nonlinear transfer function σ by the transmitter

function $\tau_i(x,y,z)$. Taking into account the cell-membrane transfer functions and summing over all of the PEs gives the complete output function *g*.

$$g(x,y,z) = \chi\left(\sum_i \sigma\left(\iiint_H h(\xi,\eta,\zeta)\, d\mu_i(\xi,\eta,\zeta)\right)\cdot \tau_i(x,y,z)\right) \tag{2}$$

The receptor measure μ_i models the shape and sensitivity the dendritic arbor in the input manifold *H*, while transmitter function τ_i models the signal distribution in the terminal arbor and the concomitant release of neurotransmitters into the output manifold *G*. The receptor measures $\{\mu_i\}$ and the transmitter functions $\{\tau_i\}$ perform the complementary operations of converting back and forth between fields defined on continuous manifolds and discrete real values resulting in both an integral and a summation sign in (2).

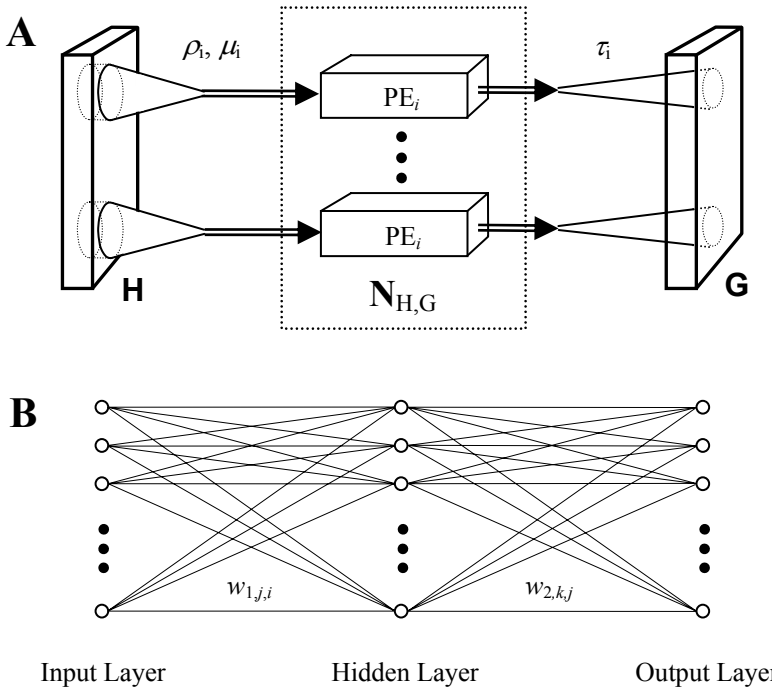

Fig. 4. A computational manifold (*A*) transforms continuous fields while a neural network (*B*) transforms discrete vectors. In the neurotransmitter field model (*A*) the Processing Elements (PE$_i$) represent neurons which are points in the function space $\mathbf{N}_{H,G}$. Since there are effectively two summations, one in the intracellular space and one in the extracellular space, the receptor measure μ, together with the transmitter function τ, allow a single layer of neurons to perform the equivalent computation of a two-layer neural network The nonlinear responses of the cell membranes separate the two summations.

2.3 Basis Functions

The continuous version of a projection neural network can be extended by generalizing the notion of radial basis functions [31] to computational manifolds. For discrete neural networks, a set of pattern vectors $\{u_\alpha\}$ and a radial basis function θ form the discriminate functions $\theta(\|u-u_\alpha\|)$. The real-valued function $\theta(x)$ has its maximum at the origin and the properties $\theta(x)>0$ and $\theta(x)\to 0$ as $|x|\to\infty$. Typically the theta functions are a Gaussian, $\exp(-x^2/2(stddev)^2$, or a similar function.

To construct the analogous continuous basis functions, we replace the discrete pattern vectors u_α with a continuous field ρ_α. Each of the functions $\rho_\alpha(\xi,\eta,\zeta)$ represents a "pattern" density defined on the input manifold. We associate a particular "target" function $g_\alpha(x,y,z)$ in the output manifold with each input pattern ρ_α. Assuming that there are several PEs available for every pattern, each PE_i is assigned a particular pattern which we label ρ_i.

The equation corresponding to a basis-function neural network can be obtained by substituting $\theta(h(\xi,\eta,\zeta)-\rho_i(\xi,\eta,\zeta))$ for h in (2)

$$g(x,y,z)=\sum_i \sigma\left(\int_H \theta(h-\rho_i)\,d\mu_i\right)\cdot\tau_i(x,y,z) \tag{3}$$

where we have omitted the variables of integration (ξ,η,ζ) for h, ρ_i, and μ_i.

Each processing element now has an additional property ρ_i, which represents the pattern to which it is the most sensitive. For each PE, the integral inside (3) is maximum when $h = \rho_i$ over the region of integration. This in turn maximizes the coefficient for the transmitter function τ_i. The sum of the transmitter functions $\{\tau_i\}$ associated with a particular input pattern ρ_α can then be defined to approximate the desired target function g_α, thereby creating the required associations.

The measures μ_i in (2) and (3) can identify the regions where the pattern ρ_i is the most sensitive. For example, we can imagine photographs of two different animals that appear very similar except for a few key features. The photographs, representing two patterns ρ_1 and ρ_2, are approximately equal, but the measures can be trained so that their value where the patterns are the same is small, but in the key regions where the patterns differ, they have much larger values. In this way, even though the two image patterns are almost the same, the output functions g_α that result from the integrals in Equation (3) could be very different.

2.4 Computational Equivalence

While models that use action potentials as state variables can form associations by using matrix operations on a large vector of neuron outputs, equation (3) shows the neurotransmitter-field state model makes it possible for a small number of neurons, even a single neuron, to establish an association between an arbitrary input pattern $\rho_\alpha(\xi,\eta,\zeta)$ and an arbitrary output pattern $g_\alpha(x,y,z)$.

A continuous computational manifold and a two-layer discrete neural network are shown in Fig. 4A and 4B. The measures $\{\mu_i\}$ in the computational manifolds can

replace the weights $\{w_k\}$ in the neural network. The corresponding summation takes place inside the cell. Since the transmitter functions $\{\tau_i\}$ can extend over a large area, even the entire output manifold, many different processing elements may contribute to the concentration of neurotransmitter at any particular point (x,y,z). Consequently, the summations in (2) and (3) are *also* equivalent to the summations in a neural network where the weights correspond to the values of the transmitter functions at a given point. This summation takes place outside the cell, as illustrated in Fig. 3. Since both the integrals with respect to the measures μ_i, and the summations over the transmitter functions τ_i, perform operations analogous to the inner product with a weight vector in a single-layer neural network, together they perform an operation analogous to a two-layer neural network.

2.5 Function Spaces

The nodes of the neural network shown in Fig. 4B are partitioned into the input layer, the hidden layer, and the output layer. In the computational manifold model shown in 4A, the input layer is analogous to the input manifold H, and the output layer is analogous to the output manifold G, where both h and g define the continuous distribution of neurotransmitters in physical space. The "hidden" layer is the space $\mathbf{N}_{H,G}$, which equals the Cartesian product of two function spaces: the space of all possible (receptor) measures on H, and the space all possible output (transmitter) functions on G. The individual neurons, PE_i, are points in this infinite-dimensional product space.

When samples of a continuous function defined on a high-dimensional space are arranged in a lower dimensional space, they will in general appear to be discontinuous. Consequently, when a collection of processing elements, $\{PE_i\}$, representing samples taken from the infinite-dimensional function space $\mathbf{N}_{H,Q}$ are arranged in three-dimensional physical space, the outputs will seem discontinuous. Moreover, realistic neural field models that attempt to describe the observed firing rates of large groups of neurons as a continuous function in physical space will be difficult or impossible to create. It may be expected that the responses of neighboring neurons will be relatively uncorrelated even when the underlying neurotransmitter fields are continuous.

2.6 Cellular Computations and Neuroglia

An abstract processing element can be defined as any cell that detects and emits a signal. In biological systems, we cannot restrict the focus to electrical signals, since even neurons detect chemical signals. Moreover, we cannot expect the behavior of neurons to be predicable if neighboring cells that use only chemical signaling are excluded from consideration.

In the central nervous system of vertebrates, there are 10 to 50 times more glial cells than neurons [2]. Astrocytes, the most common type of neuroglia, are receptive

to potassium ions and take up neurotransmitters in synaptic zones. Glial cells have also been shown to release neurotransmitters.

Unlike neurons, glial cells do not generate action potentials. Consequently, if state is encoded in the firing of neurons, glia are relegated to a support role. However, in a neurotransmitter-field model, glia can take a central position along side neurons. They may participate in both short-term and long-term memory as well as computations. However, since they lack action potentials, glial cells transmit the results of their computations more slowly.

A notable difference between a perceptron neural-network model and the neurotransmitter-field model is the speed and simplicity of learning new associations. A two-layer neural network such as the one shown in Fig. 4B typically requires an extended training phase involving repeated iterations of a back-propagation algorithm. In contrast, the neurotransmitter field model shown in Fig. 4A can learn a new association by adding a single cell, which could be a glial cell. When the new cell recognizes its image pattern, ρ_i, in the input manifold, it emits the associated neurotransmitter τ_i into the output manifold. If the new input pattern is relatively unique, previously learned associations will not be affected.

3 Association Processors

Based on neurotransmitter-field theory, we can construct a system where arbitrary collections of photographs operate as symbols. If we wish to represent numbers or letters, we can pick a font and record images of their alphanumeric glyph. Similarly, fixed-time snapshots of any two-dimensional computational map can be used as symbols representing external stimuli or motor control actions.

In Fig. 5, we show how using topological alignment, multiple input images can be combined and associated with a single output image. The ability to associate images allows us to learn the addition tables, multiplication tables or arbitrary Boolean logic operations. We therefore refer to this feed-forward system as a Λ-*map* (Λ from the Greek word *Logikos*). Like a Boolean logic gate, this computational model is stateless; its output depends only on the current value of its inputs.

The performance of image association processors quickly begins to degrade for high-resolution images when every pixel in the input image is directly used in the calculation of every output pixel. We therefore create a system with a *lattice* of processing elements where each PE takes its inputs from only a local area.

We define the *support* of PE_i to be those points in the image where the measure μ_i is non-zero. If the support of a PE is contained in a region of radius d, where d is small relative to the size of the image, we say the PE has *local support*. Although neighboring PEs will in general have overlapping regions of support, the design does not restrict the size or shape of the regions. Fig. 5 shows a PE where inputs are taken from three separate images, but each image has a different sized region of support, with one relatively "narrow", and another relatively "broad".

Transactions on Computational Science V, LNCS 5540, pp. 38–68, 2009.
M.L. Gavrilova et al. (Eds.) Springer-Verlag

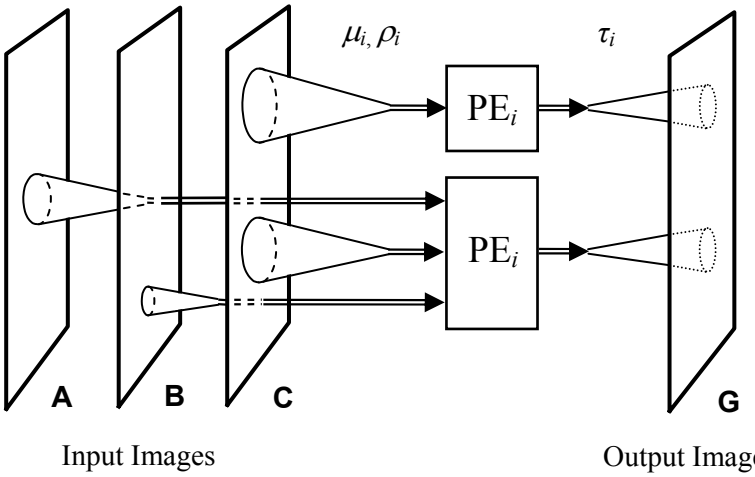

Fig. 5. The Λ-map produces an output image that is associated with multiple input images. While the input and output images are neurotransmitter fields, the model is stateless in that its current output does not depend on the previous inputs. Processing elements with local support take their inputs from small regions in multiple input images. The regions of support may be narrow as shown for image *B* or broad as shown for image *C*. The output image is produced by a lattice of PEs operating in parallel.

As shown, the output image will in general consist of a melee of uncoordinated results, with PEs in different areas recognizing different patterns. However, using recurrence the system can form numerous cyclical loops which integrate the results of the individual processing elements into a coherent overall image association.

3.1 The Psymap

Character strings that serve as symbols in a digital computer are composed of a finite sequence of bits. A binary digit is an abstract mathematical concept, which in practice, is implemented as bi-stable analog circuit. The basic unit of computer memory, the Set-Reset (SR) flip-flop shown in Fig. 6A, has two stable states corresponding to "0" and "1". Initial voltage values move along a path toward one of the two *attractors*. The set of points whose paths lead to an attractor is referred to as its *attractor basin*. Since the system must operate correctly in the presence of noise, the attractor basin must contain an open neighborhood around each *stable* fixed point. If the mathematical topology does not change under small variations of the defining parameters, the dynamical system is considered to be *structurally stable* [32]. Thus, in the physics of computer circuits, a symbol is actually a stable fixed-point-attractor basin of a dynamical system.

Internally, inside each bit of static random access memory (SRAM) is a logic circuit equivalent to the SR flip-flop shown in Figure 6A. If the *S* or *R* inputs, which

are normally one, momentarily go to zero the flip-flop will set or reset and remain there until either the *S* or *R* input is changed again. We replace the single bits *S*, *R*, *Q* and *Q'* in the SR flip-flop with two-dimensional images and we replace the two NAND gates with two Λ-maps. The resulting *psymap* is shown in Fig. 6B, where the output *Q'* has been relabeled as *P*.

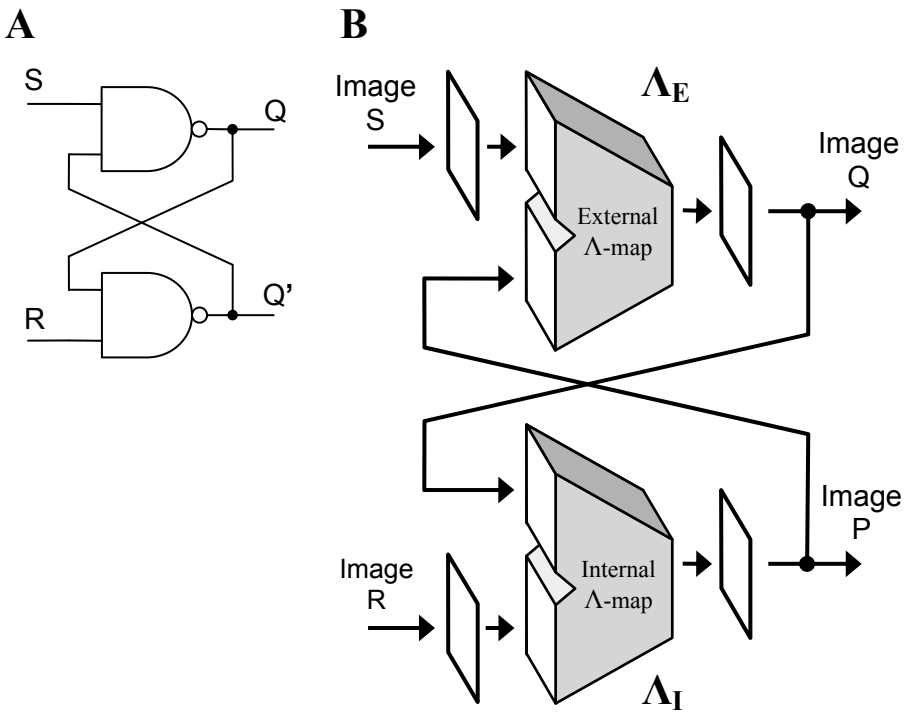

Fig. 6. The *Psymap* (*B*) is analogous to the SR flip-flop (*A*) where the bits have been replaced by images and the NAND gates have been replaced by Λ-maps. The two Λ-MAPs are labeled *External* and *Internal* and correspond to the external in internal lamina of the cerebral cortex.

Referring to the psymap in Fig. 6B, let $\Lambda_E(S, P) = Q$ denote the external Λ-map, and let $\Lambda_I(R, Q) = P$ denote the internal Λ-map. Let *Null* denote a predefined "blank" image, and let $\{(a_1, b_1), (a_2, b_2) \ldots (a_i, b_i) \ldots (a_n, b_n)\}$ be an arbitrary collection of *n* image pairs. Suppose we program Λ_E such that $\Lambda_E(Null, b_i) = a_i$ for all *i*, and program Λ_I such that $\Lambda_I(Null, a_i) = b_i$ for all *i*. When the R and S inputs are Null, the psymap will have *n* fixed-points corresponding to the n image pairs (a_i, b_i). We will refer to the images that form an image pair (a_i, b_i) as *reciprocal* images.

In addition to the above, suppose we have *n* input images $(s_1, s_2, \ldots, s_n)$ and we add the additional associations to Λ_E such that $\Lambda_E(s_i, X) = a_i$ for any image *X*. Then by changing the *S* input from Null to s_i, we can force the psymap from whatever state it is currently in to the state identified by the reciprocal image pair (a_i, b_i). If the fixed-

point is stable, when the *S* input returns to Null, the psymap will remain in this state, until either the *S* or *R* input image changes again.

In a simple feed-forward image association system with local support there is no way to coordinate the individual PE outputs to form a consistent global image association. However, the two Λ-maps which make up psymap form an image loop. The output of any particular PE feeds into the local support of several other PEs in the opposite Λ-map. These in turn form many local loops by feeding back into the original PE. Figure 7 illustrates how this can occur by showing connected PEs in two Λ-maps. This process is repeated in an interconnected mesh and is the critical step in forming global image associations using only local connectivity.

Comparing Fig. 7 with the cortical columns shown in Fig. 2, we note several analogies including the local pattern of neuron connections, the extensive number of interconnected loops, and the internal and external laminar structure.

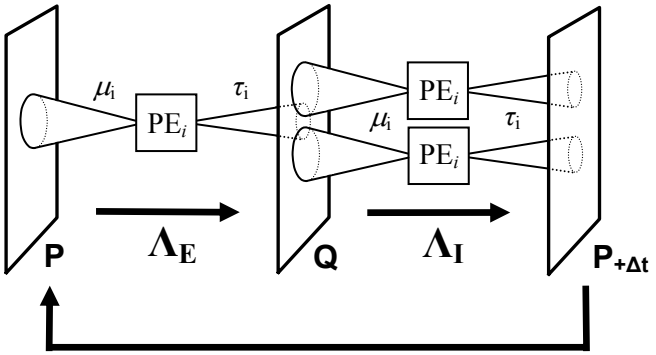

Fig. 7. The psymap computations are performed by processing elements with overlapping local input and output regions corresponding to the dendritic and axonal trees, where the image data is the neurotransmitter density. Even though each receptor measure μ_i, and transmitter function τ_i, cover only local limited areas, the recurrence allows their effect to spread over the entire image. The far right image $P_{+\Delta t}$ equals the leftmost image P following one processing cycle lasting time Δt. The pattern of interconnection closely resembles the cytoarchitecture of the cortical columns shown in Fig. 2.

In the section on experimental results, we demonstrate an implementation of the system shown in Fig. 7, which shows how local information in the input image can progressively spread to wider and wider areas as the recurrence progresses. This proves that processing elements with local support can be used to create a psymap with *stable global reciprocal-image attractors*. Consequently, since both of the associated images can be chosen arbitrarily, they can serve symbols in a cognitive system.

3.2 Receptive Fields

Recursion allows processing elements with local connections to form global associations. Varying the size of regions from which the neurons make connections, such as those shown in Fig. 5, allows a psymap to find the matching image more readily. We could "pre-compute" the average of small image regions with various sizes and use these averages as the inputs to the PEs. Rather than simply using averages, we can extend this idea by using local spectral functions such as two-dimensional wavelets.

We can associate images by associating their wavelet transforms. The spectral functions used could be identical to the receptive fields in the retina of the eye.

Axons from the *on* and *off-center ganglion cells* in the retina form the optic nerve. These cells receive inputs from nearby photosensitive rods or cones in a roughly circular *receptive field* that contains both a center area and a surrounding ring of opposite polarity. The receptive fields differ in size and are similar to spherically symmetric functions where the variation in the receptive field size is given by *s,* the *scaling* parameter [33]. The axons corresponding to the cells with large and small receptive fields remain segregated as they project to the lateral geniculate nucleus and on to the primary visual cortex (Brodmann area 17) [2], [34]. On coordinate system in the primary visual cortex, with the *z*-axis perpendicular to the surface, the size (scale) of the receptive field is topographically mapped to the z dimension. Throughout the cerebral cortex, the layers which make up the cortex have a multi-cellular thickness in the perpendicular *z* direction that gives them a three dimensional structure.

Spectral psymaps are based on the following hypothesis: The topographic mapping of receptive fields increasing in size onto the third (*z*) dimension is not an anomaly unique to visual processing, but rather, a general principle of operation that improves the efficiency and performance of the association computations throughout the entire cerebral cortex.

3.3 Wavelets

In one-dimension, a single main wavelet φ, which is normalized and symmetric about the origin, can generate a family of wavelets at position x and scale s.

$$\varphi_{x,s}(\xi) = \frac{1}{\sqrt{s}}\varphi\left(\frac{\xi - x}{s}\right) \tag{4}$$

Wavelets with a relatively large value of scaling parameter s act as low-frequency wavelets, analogous to broad areas of support, and those with a relatively small value of s act as high-frequency wavelets, analogous to narrow regions of support.

The wavelet transform of a function f is given by

$$\mathcal{W}[f](x,s) = \int_{-\infty}^{+\infty} f(\xi)\varphi^*_{x,s}(\xi)\,d\xi = \left\langle f, \varphi_{x,s} \right\rangle \tag{5}$$

where φ^* denotes the complex conjugate of φ.

Several methods are available for generating sets of multidimensional wavelets whose linear combinations are dense in $\mathbf{L}^2(\mathbb{R}^n)$. Of particular interest are spherically symmetric wavelets, which can be expressed in the form $\varphi(\mathbf{x}) = f(\|\mathbf{x}\|);\ \mathbf{x} \in \mathbb{R}^n$ for some one-dimensional function *f*. The scale parameter for spherically symmetric wavelets is a single real-valued positive number $s \in \mathbb{R}_+$. Therefore, the overall parameter space has dimension *n*+1. While some wavelets, such as the normalized second derivative of a Gaussian function, have non-zero values out to infinity, we are mainly interested in wavelets with compact support [35], in particular wavelets that are zero outside a small local region.

If a wavelet is spherically symmetric, so is its Fourier transform. Thus, $\hat{\varphi}(\boldsymbol{\omega}) = \gamma(\|\boldsymbol{\omega}\|)$ for some function γ, and the admissibility condition [9] is

$$C_\chi = \int_0^{+\infty} \frac{|\gamma(\omega)|^2}{\omega} d\omega < \infty. \tag{6}$$

For $f \in \mathbf{L}^2(\mathbb{R}^n)$ the wavelet transform, $\tilde{f}$, is defined by extending the integral in (5) to *n* dimensions. The inverse wavelet transform in *n* dimensions [36] is given by

$$f(\boldsymbol{\xi}) = \mathcal{W}^{-1}[\tilde{f}](\boldsymbol{\xi}) = \frac{1}{C_\chi} \int_{\mathbb{R}_+} \int_{\mathbb{R}^n} \tilde{f}(\mathbf{x}, s) \varphi_{\mathbf{x},s}(\boldsymbol{\xi})\, d\mathbf{x} \frac{ds}{s^{n+1}}. \tag{7}$$

Wavelet transforms on spherical surfaces are widely used in science and can be defined on other manifolds as well using the inner product [35].

3.4 Spectral Psymaps

Each of the Brodmann areas has a unique shape that projects along the perpendicular direction of the cortical columns onto a two-dimensional manifold $\mathbb{M}_i$. The spectral functions within each cortical layer are parameterized by a center position (*x*,*y*) and a single real-valued scale factor $s \in \mathbb{R}_+$. The resulting three-dimensional manifold $\mathbb{J}_i = (\mathbb{M}_i \times \mathbb{R}_+)$, maps to a single cortical layer of a single Brodmann area.

Examining the psymap shown in Fig. 7, we now replace the two-dimensional images with three-dimensional "slabs" of thickness z_0. The scaling parameter $s \in (0, \infty)$ is monotonically mapped to the interval $(0, z_0)$ that corresponds to the physical thickness of a single cortical layer in a particular Brodmann area. In the resulting three-dimensional spectral manifold, the input is now taken from a local volume where the values represent the coefficients of specific spectral functions. The PE dendritic tree spans small regions of the three-dimensional input spectral manifolds, and transmits results to a three-dimensional output spectral manifold.

Low-frequency spectral functions measure components over a large area of an image. Consequently, even though a processing element has only local connections near an image point (x_0, y_0), if the connections extend through the entire thickness of the cortical layer, its output value can change based on changes in the input image from the finest to the coarsest levels of detail. Moreover, the recursion in the psymap

allows the output values of PEs that correspond to low-frequency spectral functions to propagate quickly throughout the entire psymap.

3.5 Orthogonal Projections

Because of the scale parameter *s*, the spectral manifold on which $\mathcal{W}[f](x,y,s)$ is defined is three-dimensional. Since this spectral manifold has a higher dimension than the original two-dimensional image space, there are many spectral functions for which there is no corresponding image. Mathematically, almost all functions *h*, defined on the space of continuous wavelet transforms, do not have a well-defined inverse $\mathcal{W}^{-1}[h]$.

Consequently, the space of transformed functions is over-specified and contains redundant information. This redundancy can be used to reduce errors and make the association process faster and more efficient.

The PEs compute the required outputs for a large number of stored associations based on only limited local information. Consequently, the overall result of these calculations can only be an approximation, which may not have a well-defined inverse. However, using the *reproducing kernel* it is possible to estimate the approximation error and calculate the closest function for which the inverse spectral transformation exists.

For the one-dimensional case, the following equation defines the necessary and sufficient conditions for a function $\mathcal{W}[f]$ to be a wavelet transform [9].

$$\mathcal{W}[f](x,s) = \frac{1}{C_\varphi}\int_0^{+\infty}\int_{-\infty}^{+\infty}\mathcal{W}[f](\xi,\eta)K(x,s,\xi,\eta)\,d\xi\,\frac{d\eta}{\eta^2} \tag{8}$$

where the constant C_φ is given by (6). The reproducing kernel *K* measures the correlation between the wavelets $\varphi_{x,s}(\alpha)$ and $\varphi_{\xi,\eta}(\alpha)$ and is defined by

$$K(x,s,\xi,\eta) = \int_{-\infty}^{+\infty}\varphi_{x,s}(\alpha)\,\varphi_{\xi,\eta}(\alpha)\,d\alpha = \left\langle \varphi_{x,s}, \varphi_{\xi,\eta} \right\rangle. \tag{9}$$

Let $H = \mathbf{L^2}(\mathbb{R}\times\mathbb{R}_+)$ and let *U* denote the linear subspace of *H* where the inverse wavelet transform exists. Using the reproducing kernel specified by (9) we define the linear operator $\mathcal{V}$ by

$$\mathcal{V}[f](x,s) = \frac{1}{C_\varphi}\int_0^{+\infty}\int_{-\infty}^{+\infty} f(\xi,\eta)\,K(x,s,\xi,\eta)\,d\xi\,\frac{d\eta}{\eta^2} \tag{10}$$

From (8) we note that for $f \in U$, $\mathcal{V}[f] = f$. In a straightforward proof, it can be shown that $\mathcal{V}$ is an orthogonal projection of *H* onto *U*. If we view the local estimation errors in the calculations as additive noise $e(x,s)$, then

$$\mathcal{V}[f+e] = f + \mathcal{V}[e] \tag{11}$$

Since $\mathcal{V}$ is an orthogonal projection, $\|\mathcal{V}[e]\| \le \|e\|$. That is, $\mathcal{V}$ removes the component of the noise that is in $U^{\perp}$ and thereby projects the estimate to a function that is closer to the correct solution *f*.

This orthogonal projection can be used to increase stability in the psymap associations by reshaping the attractor basins around valid wavelet transforms where small errors result in invalid spectra, which are subsequently removed or greatly reduced by (10). When used in conjunction with a pattern recognition model based on neurotransmitter fields this projection can extend the region of stability.

From the definition of the reproducing kernel (9), we can see that at a fixed position (x_0, s_0) in the spectral manifold, the kernel $K(x_0, s_0, \xi, \eta)$ is zero for values of (ξ, η) where the spectral functions φ_{x_0,s_0} and $\varphi_{\xi,\eta}$ do not overlap. Moreover, *K* is defined in terms of the wavelets themselves and does not depend on the transformed function *f*. Consequently, the kernel *K* can be pre-computed (and encoded in the synaptic connections). The projection defined by (10) can then be evaluated dynamically at each point (*x*, *s*).

We have discussed the reproducing kernel only for the case of one-dimensional wavelets $\varphi_{x,s}$. However, the definition (9) is expressed in terms of an inner product, and in general, reproducing kernels only require the mathematical structure of a Hilbert space [37][38].

3.6 A Psymap Architecture

It is possible to design many different types of psymaps using local processing elements. Fig. 8 shows a detailed psymap design that illustrates one possible architecture. Variations of this design can achieve the same or similar functionality.

The double lines in Fig. 8 represent the transfer of data defined on three-dimensional spectral manifolds. The letter $\mathcal{G}$ denotes a general association operator such as the lattice of processing elements shown in Fig. 4A, the letter $\mathcal{V}$ denotes orthogonal projections based on the reproducing kernel, and the vertical box marked $\mathcal{M}$ performs multiplexing operations based upon the mask inputs marked T_S and T_R. Each box labeled $\mathcal{G}$ is trained with a different set of input and output relationships and consequently carries a subscript that identifies it as a unique transform.

The inputs, $\{s_k\}$ and $\{r_k\}$, represent collections of image spectra that arise from either subcortical regions or from the outputs of other Brodmann areas. The integration of data from three separate input images was illustrated in Fig. 5. If $\mathcal{G}_S$ (or $\mathcal{G}_R$) forms the same output association for several members of a given collection of inputs $\{s_i\}$ (or $\{r_i\}$), then the associations will mutually reinforce one another. Consequently, even though single inputs may not be sufficiently strong to bring forth a recollection, multiple inputs will add "context", and their combined effect may surpass a threshold required to evoke the entire memory.

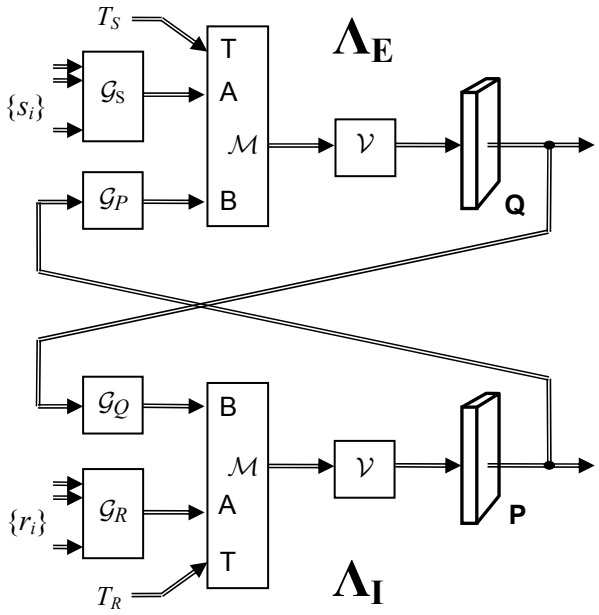

Fig. 8. A detailed psymap implementation illustrates the general pattern of interconnection. $\mathcal{G}$ denotes a neural network association operation, $\mathcal{M}$ denotes the masking and multiplexing operation and $\mathcal{V}$ denotes the orthogonal projection based on the reproducing kernel.

The multiplexer masks allow the system to focus attention on selected regions and to control whether individual Brodmann areas accept new inputs or retain their current contents. Each of the reciprocal Λ-maps, shown in Fig. 8, contains two separate, association elements whose outputs feed into the *A* and *B* inputs of the multiplexer box labeled $\mathcal{M}$. A third input, labeled *T*, shown with a diagonal line, is the control mask.

Let $\alpha(x, y, s)$ be one of the mask signals T_S or T_R. These can control the multiplexer by performing an operation analogous to the *alpha blending* calculation, $(1-\alpha)A + \alpha B$, used for image composition in computer graphics [39]. For points where $\alpha = 0$, the output equals *A*, and where $\alpha = 1$, the output equals *B*. Values in between smoothly blend the two images.

When the spectral coefficients are not based on a set of orthogonal functions, the result of an association formed by a real-valued neural network will usually contain small errors that result in invalid spectral representations. Moreover, the masking operation may also result in a spectral function that does not correspond to the transform of an actual image. However, using the reproducing kernel (9) we can project these functions using the linear operator $\mathcal{V}$ given by (10) to the nearest function for which the inverse transform $\mathcal{W}^{-1}$ produces a valid result. This operation is shown in Fig. 8 following the multiplexing operation. Since the results of the orthogonal

projections are Q and P, we thereby guarantee that the spectral outputs of a psymap always correspond to valid images.

As long as the control signal $\alpha(x, y, s)$ is identically equal to one, in both the exterior and interior Λ-maps, the psymap will ignore its inputs and retain its current stored value. Under these conditions, the psymap is *latched* and the contents of this short-term memory remain fixed on the outputs Q and P.

4 The Psymap Array Model

If each Brodmann area corresponds to a unique psymap, then the collection of all the Brodmann areas in the cerebral cortex constitutes a *psymap array*.

A graphic representation of a psymap array is shown in Fig. 9 where the lines denote the transfer of complete images. To simplify the diagram, we use an "I/O Bus" notation where the horizontal rows along the top of the diagram represent the images, and dots are used to illustrate connections. Sensory inputs are transmitted as computational maps, as are the motor control outputs. Each psymap generates two output images, corresponding to the two component Λ-maps. Physiologically, the two output images arise from the exterior and interior pyramidal layers of the cortex. These are connected figuratively via the I/O bus to other areas. Each psymap can have any number of images as inputs, which are integrated together using topographic alignment.

Each psymap in the psymap array corresponds to a unique Brodmann area. The number and source of the inputs and the number of associations formed will vary between psymaps and even between the internal and external Λ-maps of a single psymap. These variations will affect the computational requirements of the different cortical layers causing them to vary in thickness between Brodmann areas. However, within a single Brodmann area, the number of associations and the type and origin of the inputs will be the same throughout, suggesting that the thicknesses of the layers should be approximately the same. Thus, the psymap array model predicts the observed sharp transitions between Brodmann areas and a uniform thickness within each area [1].

Brodmann mapped the cortical regions of many mammals [40] including those of the monkey in diagrams similar to the one shown in Fig. 10. These drawings can be directly correlated with the psymap array model such as the one shown in Fig. 9.

An assumption underlying some cognitive models is that during the course of evolution, there was a sudden "break" when the CNS developed a new type of feature extraction mechanism that converted images into tokens, instances taken from a small finite set of discrete symbols. It was then able to manipulate these tokens using a new symbolic processing engine that simultaneously evolved during this same time interval. An alternate hypothesis is that this "break" never took place. Instead, additional general-purpose image association processors, computational engines that had already evolved, were replicated to solve problems of increasing difficulty. Most recently, during the last few million years, the already existing psymap array expanded

again, adding and integrating new psymaps for language and other aspects of abstract reasoning [41].

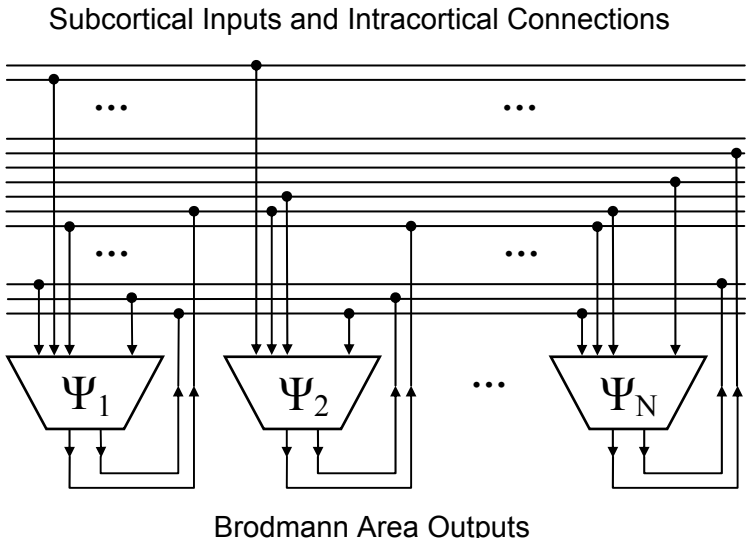

Fig. 9. The psymap array model of the cerebral cortex. Each psymap, Ψ_i, corresponds to a separate Brodmann area. Lines in the diagram correspond to images, and dots represent specific input and output connections.

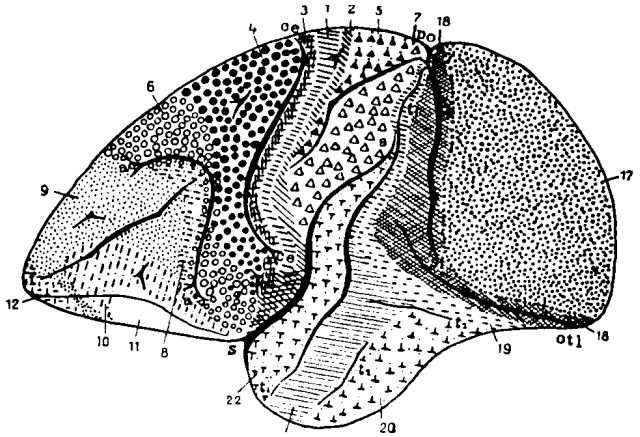

Fig. 10. The Brodmann areas of the monkey cortex. The general principles of operation of a psymap array model can be applied to describe the cerebral cortex of any mammal.

Transactions on Computational Science V, LNCS 5540, pp. 38–68, 2009.
M.L. Gavrilova et al. (Eds.) Springer-Verlag

4.1 Attention and Control

Inside every CPU, a control unit coordinates the flow of data between the various components. Every area of the neocortex has reciprocal connections with the thalamus [42], which is known to play an important role in consciousness. Based on observed behavior and the types of real-world problems that the CNS must solve, an agile and flexible control mechanism would be based on image subsets or regions. As a first approximation, we can view these image regions as "control masks" that overlay the psymap and regulate the psymap processing and Input/Output. These masks are the T_S or T_R. control images that are shown as inputs to the multiplexer in Fig. 8. The masks blanket the entire extent of the psymap "content" images and consequently can be used to identify an arbitrary region within the image. The portions of the images inside the masked region are active while those outside of the region are quiescent.

In this way the thalamus can focus attention on the entire image or on some very small detail. Given the variety of computational maps, control masks can be used to direct our attention to a small region in the visual field, a single sound in a word, a particular part of the body surface, or the motion of a single muscle. Time varying control masks can be used to spatially scan a visual image, or temporally scan through the sounds of a sentence.

5 Stability

Frequency domain techniques increase the performance and efficiency of psymaps, but are not required for their stability. The analysis described in this section, and demonstrated experimentally in the next, can be directly applied to scalar or vector valued functions defined on a manifold of any dimension, with or without the use of spectral transformations.

The partial differential equations that describe the behavior of reciprocal-image attractors over time constitute an infinite-dimensional dynamical system [43]. However, some basic principles can be illustrated in a vastly simplified system, which can be generalized to construction and analysis in higher dimensions. In particular, we analyze the behavior of a psymap composed of two black-and-white single-pixel images. This very simple psymap can be expressed by two mutually recurrent equations $y = f(x)$ and $x = g(y)$ where x and y are real numbers. For one-pixel images, the integral in (3) becomes the evaluation of θ at a single point and transmitter functions, τ_i, become real-valued constants which we can as label x_i and y_i. We set σ to the identity function. Using two recursively connected PEs, we can create a fixed point at an arbitrary location (x_0,y_0) with the two Gaussian θ functions

$$\begin{aligned} y &= f(x) = y_0 \exp\left(-(x - x_0)^2 / c_x^{\,2}\right) \\ x &= g(y) = x_0 \exp\left(-(y - y_0)^2 / c_y^{\,2}\right). \end{aligned} \tag{13}$$

It is easy to verify that (x_0,y_0) is a fixed point of (13). The two equations can be combined, $x_{+\Delta t} = g(f(x))$, and differentiated to verify that the fixed point is stable. This can be seen graphically in Fig. 11A. The arrows indicate steps in the recursion (13), which moves toward the stable fixed-point located at the intersection of the two curves. Because the derivatives of *f* and *g* are zero at the fixed-point, the convergence is *superlinear*, that is, the rate of convergence increases without bound as the recursion approaches the stable attractor.

In Fig. 11B we show the characteristics of a single-pixel psymap with a total of four processing elements, two processing elements in each of the two Λ-maps. In the neurotransmitter field summation (3), the two PEs generate bimodal functions that contain two bell-shaped Gaussian curves. By setting the ρ_i and τ_i. values of each PE – which correspond to x_0 and y_0 in (13) – we can create two stable reciprocal attractors at arbitrary locations (x_1,y_1) and (x_2,y_2). The attractor basins are shown as shaded areas on the *x* and *y* axes in Fig 11B. Within these regions, the psymap will converge toward the stable attractors, as it does in the system shown in Fig 11A.

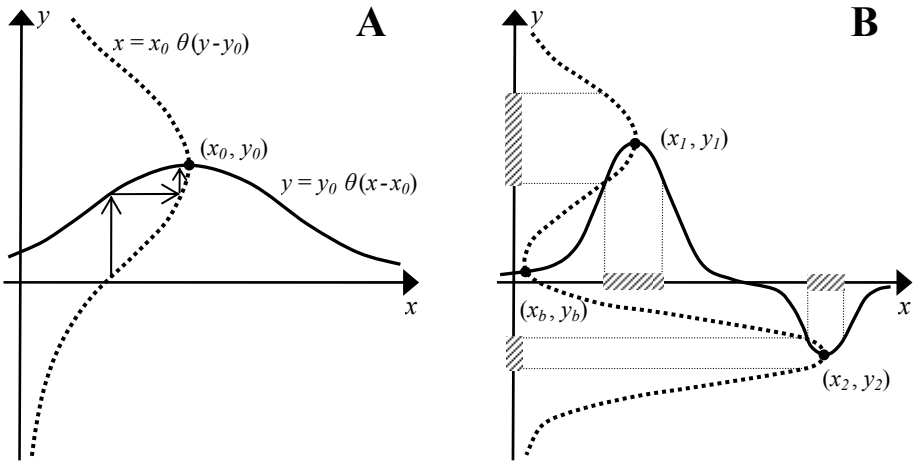

Fig. 11. The recursive equations defined by real-valued Gaussian theta functions (13) create a stable fixed-point attractor at (x_0, y_0) in the system (*A*). The arrows, which illustrate successive iterations of the recurrence, describe the behavior of a psymap for images near a reciprocal-image attractor. Two stable attractors can be created (*B*) with two processing elements in each Λ-map. The attractor basins are delineated by shaded regions on the *x* and *y* axes.

The curves shown in Fig 11B intersect in five locations; therefore, the system has five fixed-points. Two of these are unstable, but there is a *third stable* fixed-point located near the origin and labeled (x_b,y_b). This point corresponds to a pair of nearly black (zero-valued) reciprocal-images. This stable fixed-point will occur when none of the processing elements "recognizes" the zero input values, which in turn causes the summation of their outputs in both Λ-maps to be nearly zero. When started from

initial values outside of the shaded areas shown, the association will "collapse" and the system will converge to the near-zero value (x_b,y_b).

Because of their non-zero tails, the two Gaussian theta functions will to some extent overlap, which may cause an unwanted "association skew" in the two Λ-maps. This effect can be minimized by setting the standard deviation to a small value. Moreover, bell-shaped theta functions can be created which have compact support, that is, functions that are identically equal to zero outside some finite closed interval.

By decreasing the width of the Gaussian theta functions, new stable attractors can be created by including one additional PE in each of the Λ-maps. As long as their x and y positions do not overlap with an existing attractor, the new attractors can be placed in arbitrary locations. Initial values near any of the reciprocal-image attractors will exhibit a convergence comparable to the system illustrated in Fig. 11A. Physiologically, this implies that we can create a new "memory", that is a new stable attractor, with only two neurons (or glial cells), one in each Λ-map.

The basic principles described for a single-pixel scalar-valued psymap can be generalized to higher dimensions. Many interdependent factors, such as the restriction of the receptor (μ_i) and transmitter (τ_i) functions to local regions, generate complex behavior and confound the analysis. However, while the resulting systems may have any number of periodic or chaotic attractors, it is possible to create local neighborhoods where the psymaps are structurally stable.

We can imagine a large geographic area with attractor basins created by the force of gravity where a frictionless ball would roll into valleys or "energy wells". The attractors correspond to the local minimum in each valley. The ability to specify the ρ_i, μ_i and τ_i functions in (3) in addition to the θ and σ characteristics provides a great deal of flexibility in controlling the potential energy landscape. The patterns control the positions of the valleys, and the theta and sigma functions control the size and the steepness of the sides. Decreasing the size of the energy wells allows the image association capacity to be increased without limit. The smaller attractor size may make the associations more difficult to "find", but once located, the attractors will be stable.

Using multiple psymaps is a potentially very powerful technique since it can serve as a mechanism to trigger a "recognition cascade" where convergence in one or more psymaps causes a cascade of convergence in several others. This is possible since each psymap can accept input images from many other Brodmann areas. Again using the metaphor of gravity and geographical landscapes, each psymap has its own landscape. While we may be searching for a relatively tiny reciprocal-image attractor in one, another psymap may have a large expansive valley where convergence toward the bottom, brings us closer to the precise solution in the first psymap. This phenomenon is well known and well studied in psychology, where verbal "hints" about what an image contains help us locate it. Crossword puzzles are an example of multi-sensory integration, where phonetic sounds are combined with semantic meaning to help find the correct association. As soon as it is located, the association itself is very stable.

6 Experimental Results

A software package written in Java [44] was used to test a variety of psymaps where the data values ranged from single pixels to functions defined on one, two and three dimensional manifolds. In all cases, stable attractors were created analogous to those shown in Fig. 11A and 11B. Consequently, while the results demonstrated are limited to two-dimensional images, similar stable behavior generalizes to spaces of arbitrary dimension which may or may not include frequency components such as those produced by a wavelet transform.

A system with eight stable attractors was constructed from the eight image pairs shown in Fig. 12.

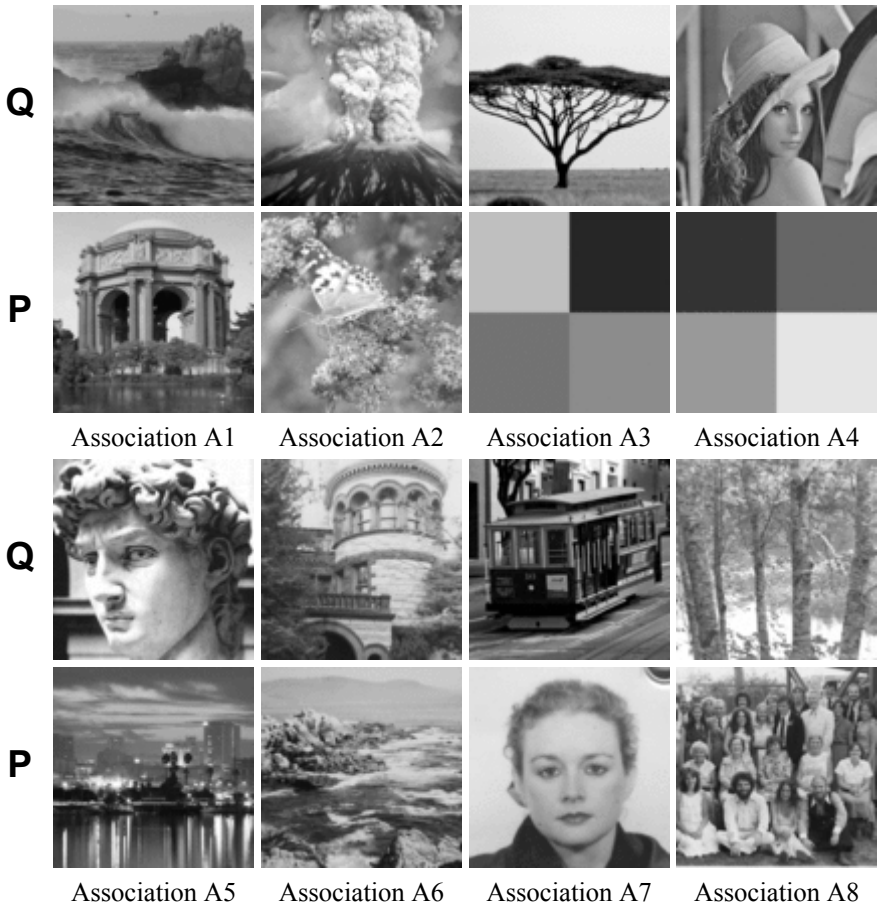

Fig. 12. The sixteen associated images used to construct a single psymap that contained eight reciprocal-image attractors.

Figures 13, 14 and 15 illustrate the convergence of the psymap to one of the stable reciprocal-image attractors. In each experiment the initial value is shown as the leftmost image *Q*. In Fig. 13, the photograph of the volcanic eruption obscured by various lines and circles represents a displacement away from the fixed-point attractor corresponding to association A2, but still within its attractor basin. The iterated sequence of images shows the image pair moving toward the stable fixed-point. In Fig. 14, the photograph of "Lena" obscured by the same lines and circles converges instead to the association A4. In Fig. 15, the initial value consists of random circles and line segments added to the Lena test image.

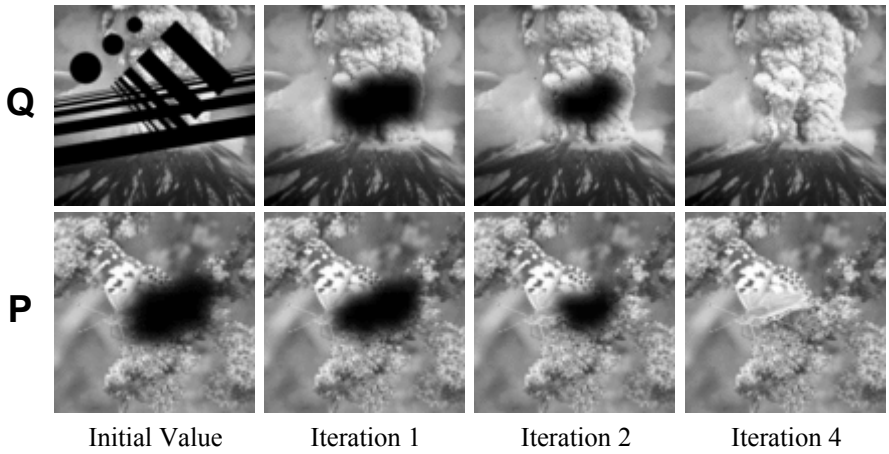

Fig. 13. An initial value that converges to the association A2 reciprocal-image attractor.

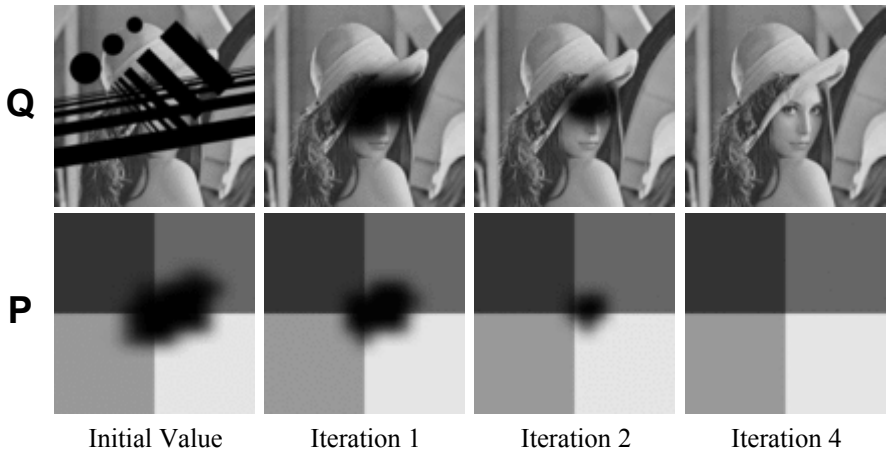

Fig. 14. An initial value that converges to association A4. Creating an association with a square "barcode" image pattern helps assist in recognition and classification.

Image pixels effectively correspond to synapses rather than neurons. Consequently for equivalent image resolutions, the processing time and the training time are much less than the corresponding neural network model. In the test case shown, the image resolution was 256×256 but the PEs were spaced 16 pixels apart, resulting in a total of (16+1)×(16+1) PEs. The size of the receptor regions was 64×64 pixels and the transmitter regions were 48×48 pixels. Thus, associations between two 65,536-pixel images were created with 289 PEs where each PE had a localized receptor region of 4,096 pixels.

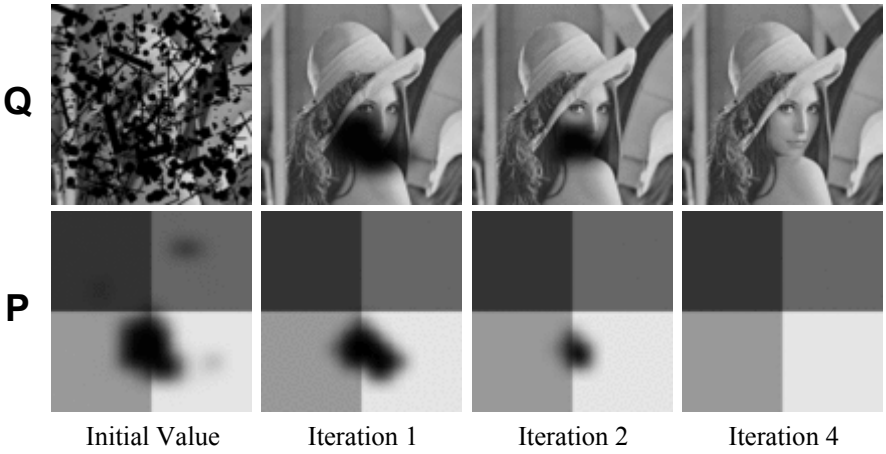

Fig. 15. An initial value obscured by numerous random lines and circles that also "collapses" locally in some areas, but is still within the global attactor basin of association A4.

The training phase consisted of creating a mesh of PE objects whose overlapping receptor and transmitter regions covered the input and output images respectively. For each image association, a new set of PEs was created and added to the system.

To create a smooth transition between regions the transmitter functions were initialized with a two-dimensional "hill-shape" before scaling by the adjusted output image. The transmitter function, τ_i, of each PE has a significant non-zero multiplier only when an image close to the associated pattern ρ_i is present on the input. Consequently, since each pixel is contained in several overlapping regions, the training phase consists of scaling all the τ_i functions, whose PEs have the same input pattern, so they sum to the desired output pixel values. To calculate the τ_i, all of the two-dimensional hill-shaped initial values are summed pointwise resulting in an image that represents the size and extent of the overlap in the transmitter regions. A scalar coefficient for each pixel is then calculated by dividing the desired image by this summed image. The scalar coefficients are then multiplied pointwise by each of the initial transmitter values, which respond to that input pattern, resulting in a set of transmitter functions whose sum will equal the associated output image. Thus, the initial transmitter regions can have arbitrary size and shape as long as they collectively cover the output manifold.

All of the images used had a resolution of 256×256 pixels, but the processing element grid was only 17x17. Since the computations are primarily inner products and summations, they execute quickly and are suitable for parallel implementations. For the results shown, the set-up time was less than 10s and the run time for each of the tests was approximately 30s on a single processor 2 GHz personal computer.

The training and execution times are a significant improvement over common neural-network algorithms for several reasons related to the fundamental differences in the computational models. During the set-up or training phase, time-consuming back propagation methods are not required since learning takes place by adding cells which recognize an input image, and directly generate the associated output image. In the neurotransmitter-field model, neither the training phase nor the testing phase uses a slow (and often error prone) minimization algorithm. Moreover, as was discussed in section 5, the convergence rate near the fixed-point attractor is superlinear. The execution time is also faster since an action potential does not correspond to the value of a single pixel, but rather acts as a signal to all of the synapses in an axonal tree which define the image values over an entire region.

The rate and nature of the convergence shown in Figs 13-15 can be modified by changing the standard deviation of the theta functions, as well as the slope and inflection point of the sigma functions. Small values of the standard deviation for θ prevent interference between image associations. For the results illustrated, a modified hyperbolic tangent function was used for sigma transfer function with the inflection point at 0.15 and the slope at the inflection point equal to 40. If the inflection point for σ were set to a relatively large value such as 0.75, then more than 75% of the pixels in each PE receptor region μ_i would have to match (approximately) to produce a coefficient for τ_i of greater than 0.5. In this case, the initial values used in the test cases would diverge to all black images. Additional experimental results with automatically generated HTML reports, which document the parameter settings and computed outputs, are available online [45].

Locally, many of the characteristics of single-pixel psymaps, illustrated in Fig 11, also apply to psymaps defined on multi-dimensional manifolds. For example, in the associations A3 and A4, both of the *P* images are square "barcode" images. However, because the grayscale values differ, the associations remain separated as they do for the fixed-points (x_1,y_1) and (x_2,y_2) in Fig. 11B. The test results also show how in some local regions, there are insufficient matching pixel values, causing the association to collapse and move toward the all black (x_b,y_b) fixed-point.

A central concept, which all three experiments help illustrate, is that global system behavior can be generated from the purely local action of neurons. In both training and operation, each PE only has access to information in its own receptor and transmitter regions. However, the neighboring cells interact to re-establish the missing local details. The recurrence in the overlapping regions of support make it possible for the local connections to establish overall global associations.

Conclusions

The stability of the computation results demonstrates that it is possible to associate arbitrary images rather than discrete bit patterns in the construction of a general-purpose symbolic processor. However, additional study is required in several areas. From the purely mathematical point of view, psymaps and psymap arrays are interesting but complicated objects. Images are defined in infinite-dimensional function spaces, and determining the characteristics of the attractor basins, as well as the behavior of the system when external (sensory) input images are constantly changing, is important but difficult. From a computational perspective, the effectiveness of local spectral representations and the orthogonal projection using the reproducing kernel must be measured and analyzed. Finally, and most important, the validity of the model as a scientific explanation needs to be established or refuted. The theory presented contains several interrelated propositions, which include the neurotransmitter cloud hypothesis and the existence of reciprocal-image attractors in the cerebral cortex. The current lack of contradicting scientific facts cannot be construed as a strong supporting argument, and it seems likely that targeted biological experiments will be required.

The psymap is a new type of image centric processing architecture, which combines several design elements including recurrence of locally connected processing elements, spectral transformations, and an orthogonal projection based on the reproducing kernel. Compared to a neuron action-potential model, a neurotransmitter-field model presents a broader view of natural intelligence. It allows the chemical reactions that take place in many types of cells, including neuroglia, to be incorporated into a general framework of memory and computation. Direct associations between images are shown to be stable, and therefore the images themselves can act as symbols. The psymap array model has many correlations with the neurological organization of the cerebral cortex and may help provide insight into the nature of consciousness and cognition.

Acknowledgments. The author would like to thank Professor M. Tuceryan for his support and helpful comments. This document contains material that is patent pending by General Manifolds LLC, http://www.gmanif.com/ip.

References

1. Brodmann K.: Vergleichende Lokalisationslehre der Grosshirnrinde in ihren Prinzipien dargestellt auf Grund des Zellenbaues. Barth, Leipzig (1909)
2. Kandel, E.R., Schwartz J.H., Jessell T.M.: Principles of Neural Science. (4th ed.) McGraw-Hill, New York (2000)
3. Garoutte B.: Survey of Functional Neuroanatomy. (3rd ed.) Mill Valley Medical, California (1994)
4. Spivak M.: A Comprehensive Introduction to Differential Geometry (3rd ed.), Publish or Perish, Wilmington (1979)

5. Schutz B.: Geometric Methods of Mathematical Physics. Cambridge University Press, Cambridge (1980)
6. Knudsen E.I., du Lac S., Esterly, S.D.: Computational Maps in the Brain. Ann. Rev. of Neuroscience, vol. 10, pp. 41-65 (1987)
7. Greer D.S.: A Unified System of Computational Manifolds. Tech. Rep. TR-CIS-0602-03, Dept. of Comp. and Info. Sci., IUPUI, Indianapolis (2003)
8. Monad, J.: Chance and Necessity: An Essay on the Natural Philosophy of Modern Biology (Trans. A. Wainhouse). Knopf, New York (1971)
9. Mallat S.: A Wavelet Tour of Signal Processing. (2nd ed.) Academic Press, San Diego (1999)
10. Wang Y.: The Cognitive Processes of Abstraction and Formal Inferences. Proc. 4th IEEE International Conf. on Cognitive Informatics, Irvine, California (2005)
11. Wang Y.: The Theoretical Framework of Cognitive Informatics. International J. of Cognitive Informatics and Natural Intelligence, 1(1), pp. 1-27, (2007)
12. Yao, Y.Y.: Concept Formation and Learning: a Cognitive Informatics Perspective. Proc. 3rd IEEE International Conf. on Cognitive Informatics, Victoria, Canada (2004)
13. Prince, V., Lafourcade M.: Mixing Semantic Networks and Conceptual Vectors Application to Hyperonymy. IEEE Trans. Systems, Man and Cybernetics, C, vol. 36. pp. 152-160 (2006)
14. Willshaw D.J., Buneman, O.P., Longuet-Higgins, H.C.: Non-holographic Associative Memory. Nature, Vol. 222, pp. 960-962 (1969)
15. Kosko, B.: Bidirectional Associative Memories. IEEE Trans. Systems, Man and Cybernetics, vol. 18, pp. 49-60 (1988)
16. Xu, Z., Leung, Y., He, X.: Asymmetrical Bidirectional Associative Memories. IEEE Trans. Systems, Man, and Cybernetics, vol. 24, pp. 1558-1564, (1994)
17. Chua, L.O., Yang, L.: Cellular Neural Networks: Theory," IEEE Trans. Circuits and Systems, vol. 35(10), pp. 1257-1272 (1988)
18. Zhang, Q., Benveniste, A.: Wavelet Networks. IEEE Trans. Neural Networks, vol. 3 (6), pp. 889-898 (1992)
19. Thuillard, M.: A Review of Wavelet Networks, Wavenets, Fuzzy Wavenets and their Applications," in Advances in Computational Intelligence and Learning: Methods and Applications. Kluwer, Deventer (2002)
20. Iyengar, S.S., Cho, E.C., Phoha, V.V.: Foundations of Wavelet Networks and Applications. CRC, Boca Raton (2002)
21. Beurle, R. L.: Properties of a Mass of Cells Capable of Regenerating Pulses. Philosophical Trans. of the Royal Society. Series B, vol. 240. pp. 55-94 (1956)
22. Griffith, J. S.: A Field Theory of Neural Nets: I: Derivation of Field Equations. Bulletin of Mathematical Biophysics, vol. 25. pp. 111-120 (1963)
23. Griffith, J. S.: A Field Theory of Neural Nets: II. Properties of the Field Equations. Bulletin of Mathematical Biophysics, vol. 27. pp. 187-195 (1965)
24. Amari, S.: Dynamics of Pattern Formation in the Lateral-Inhibition Type Neural Fields. Biological Cybernetics, vol. 27. pp. 77-87 (1977)
25. Ermentrout, B.: Neural Networks as Spatio-temporal Pattern-Forming Systems. Reports on Progress in Physics, vol. 61. pp. 353-430 (1998)
26. Vogels, T. P., Rajan, K., Abbott, L. F.: Neural Network Dynamics. Annual Rev. Neuroscience, vol. 28. pp. 357-376 (2005)
27. Sarnat, H. B., Netsky, M. G.: Evolution of the Nervous System. (2nd ed.) Oxford (1981)
28. Widrow, B., Hoff, M. E.: Adaptive Switching Circuits. WESCON Convention Record, IRE, New York pp. 96-104 (1960)
29. Royden, H. L.: Real Analysis (3rd ed.) Prentice-Hall, Englewood Cliffs (1988)
30. Greer, D.S.: Neurotransmitter Fields. Proc. of International Conf. on Artificial Neural Networks, Porto, Portugal, (2007)

31. Bishop, C. M.: Neural Networks for Pattern Recognition. Oxford University Press, (1995)
32. Thompson, J.M.T., Stewart, H.B.: Nonlinear Dynamics and Chaos. Wiley, Hoboken (2002)
33. Nevatia, R.: Machine Perception. Prentice-Hall, Englewood Cliffs (1982)
34. Churchland, P., Sejnowski, T.J.: The Computational Brain. MIT Press, Cambridge 1994.
35. Daubechies, I.: Ten Lectures on Wavelets. Society for Industrial and Applied Mathematics, Philadelphia (1992)
36. Addison, P.S.: The Illustrated Wavelet Transform Handbook. Institute of Physics Publishing, Bristol (2002)
37. Aronszajn, N.: Theory of Reproducing Kernels. Trans. of the American Mathematical Society, vol. 68 (3), pp. 337-404, (1950)
38. Saitoh, S.: Integral Transforms, Reproducing Kernels and their Applications. Addison Wesley Longman, Essex (1997)
39. Thompson, K.: Alpha Blending. In: A. Glassner (Ed.), Graphics Gems, pp 210-211, Academic Press, Cambridge (1990)
40. von Economo, G. N. Koskinas, G.N.: The Cytoarchitectonics of the Adult Human Cortex, (trans. H. L. Seldon), Springer, Heidelberg (1925)
41. Greer D.S.: The Computational Manifold Approach to Consciousness and Symbolic Processing in the Cerebral Cortex. Proc. 7th IEEE International Conference on Cognitive Informatics. (2008)
42. Behrens, T.E.J., Johansen-Berg, Woolrich, H.M.W., Smith, S.M., Wheeler-Kingshott, C.A.M., Boulby, P.A., et al.: Non-invasive Mapping of Connections between Human Thalamus and Cortex Using Diffusion Imaging. Nature Neuroscience, vol. 6 (7), pp. 750-757 (2003)
43. Robinson, J.C.: Infinite-Dimensional Dynamical Systems: An Introduction to Dissipative Parabolic PDEs and the Theory of Global Attractors. Cambridge University Press (2001)
44. Greer D.S.: Sapphire 0.4 Implementation Notes. Tech. Rep. TR-CIS-0714-08, Dept. of Comp. and Info. Sci., IUPUI, Indianapolis (2008)
45. Computational Results, `http://www.gmanif.com/results.html`

Transactions on Computational Science V, LNCS 5540, pp. 38–68, 2009.
M.L. Gavrilova et al. (Eds.) Springer-Verlag